



Inelastic scattering of 14.1 MeV neutrons on iron

N. A. Fedorov^{1,2,3,a}, D. N. Grozdanov^{1,4}, Yu. N. Kopatch¹, T. Yu. Tretyakova^{1,2,3}, I. N. Ruskov^{1,4}, V. R. Skoy¹, I. D. Dashkov^{1,2,3}, F. A. Aliyev^{1,5}, S. Dabylova^{1,6}, C. Hramco^{1,7}, A. Kumar⁸, A. Gandhi⁸, D. Wang⁹, E. P. Bogolyubov¹⁰, D. I. Yurkov¹⁰, TANGRA collaboration

- ¹ Joint Institute for Nuclear Research (JINR), 141980 Dubna, Russia
² Faculty of Physics, Lomonosov Moscow State University (MSU), 119991 Moscow, Russia
³ Skobeltsyn Institute of Nuclear Physics, Lomonosov Moscow State University (SINP MSU), 119991 Moscow, Russia
⁴ Institute for Nuclear Research and Nuclear Energy (INRNE) of Bulgarian Academy of Sciences (BAS), 1784 Sofia, Bulgaria
⁵ Institute of Geology and Geophysics (IGG), AZ1143 Baku, Azerbaijan
⁶ L.N. Gumilyov Eurasian National University, 010000 Nur-Sultan, Kazakhstan
⁷ Institute of Chemistry, Academy of Science of Moldova, 2001 Chisinau, Republic of Moldova
⁸ Banaras Hindu University, 221005 Varanasi, India
⁹ Xi'an Jiao Tong University, Xi'an 710049, China
¹⁰ All-Russia Research Institute of Automatics (VNIIA), 127055 Moscow, Russia

Received: 7 September 2020 / Accepted: 23 May 2021 / Published online: 15 June 2021
© The Author(s), under exclusive licence to Società Italiana di Fisica and Springer-Verlag GmbH Germany, part of Springer Nature 2021
Communicated by Navin Alahari

Abstract An investigation of inelastic scattering of 14.1 MeV neutrons on an iron sample was carried out using an improved TANGRA (TAGged Neutron and Gamma RAYs) setup at JINR (Dubna). The yields of the occurring γ -transitions and anisotropy of the emitted γ -rays were measured using the tagged neutron method. The setup with a high-purity germanium (HPGe) detector was used to obtain the energy spectrum of γ -rays. The setup with 18 BGO scintillation detectors positioned in a circle around the sample was used to obtain angular distributions of γ -rays. A detailed γ -spectrum for $(n, X\gamma)$ reactions was obtained and the γ -ray angular distribution was measured for the 847 keV and 1238 keV γ -transitions. The distribution was fitted by Legendre polynomials up to fourth order and the angular distribution coefficients a_2, a_4 were extracted. A comparison with other published experimental results is given. Model calculations using computer code TALYS 1.9 were performed. The results of calculations are discussed in comparison with the obtained experimental data.

1 Introduction

The study of inelastic neutron scattering is important from the fundamental science point of view and is necessary for the nuclear physics practical applications. Despite the long history of the issue, the constant development of technology

requires a refinement of the nuclear data. In recent years, precisely measured cross-sections and yields of the processes taking place in fast neutrons scattering have gained particular relevance in connection with the development of the Generation-IV nuclear reactors.

One of the most important tasks is obtaining data for iron isotopes. Iron is a component of stainless steel, which is used as a structural material in a wide variety of fields, including nuclear energy and physical research. The natural composition of iron isotopes consists of ^{56}Fe (91.75%), the other stable isotopes make a significantly smaller contribution: ^{54}Fe (5.85%), ^{57}Fe (2.12%), and ^{58}Fe (0.28%) [1]. The importance of their nuclear characteristics for both nuclear engineering and nuclear physics leads to a high demand on actual data. The cross-sections of neutron inelastic scattering on ^{56}Fe are needed in the Nuclear Data High Priority List [2]. The nuclide ^{56}Fe and Fe-minor isotopes have been included in the CIELO international collaboration research program to improve the evaluated nuclear data files of the major nuclides [3].

The scattering of fast neutrons by iron and neutron-induced γ -radiation was extensively studied, starting with pioneering work in 1935 [4]. The measurement of the γ -quanta production cross-section and determination of the γ -ray angular distribution, primarily for the first transition in ^{56}Fe ($E_\gamma = 846.8$ keV), has been the subject of many experiments performed at various neutron energies. In recent years, most experiments, along with improving data accuracy, are aimed at conducting measurements in a wide range of neutron

^a e-mail: na.fedorov@physics.msu.ru (corresponding author)

energies to test the results of nuclear reaction model simulations. A high-resolution measurement of the γ -transitions cross-sections on iron for several incident neutron energies E_n in the range from 6.5 up to 64.5 MeV was done at CNL [5], and for E_n from 0.1 to about 18 MeV at JRC-Geel [6, 7]. At the *n*ELBE neutron time-of-flight facility, the cross-sections for E_n from 0.8 to about 9.6 MeV and the angular distribution of the γ -quanta, emitted in inelastic neutron scattering for E_n from 0.1 to 10 MeV, were investigated [8, 9]. The recent measurements of the inelastic scattering cross-section and γ -ray angular distributions were performed at the University of Kentucky [10] for several incident energies E_n from 1.30 to 7.96 MeV.

Previously, a significant part of the experiments was performed using monoenergetic 14 MeV neutrons [11]. Due to the compactness of 14 MeV neutron sources, the fast neutron scattering reaction is widely used for applied research [12]. Theoretical and model descriptions of the neutron inelastic scattering require a precise measurement of the cross-sections and n - γ correlations. γ -quanta emission cross-sections are needed for fast elemental analysis; γ -quanta angular distributions could be used to improve the accuracy of an elemental composition determination. The existing database on the angular distributions of γ -rays emitted during the neutron inelastic scattering process contains contradictory information and quite scattered values at large and small angles.

As part of the TANGRA international collaboration, at Frank Laboratory of Neutron Physics of the Joint Institute for Nuclear Research (FLNP JINR) a facility was created for studying the inelastic interaction of 14.1 MeV neutrons with atomic nuclei using the Tagged Neutron Method (TNM) [13, 14]. Based on the experience from the previous experiments on the inelastic neutron scattering by other nuclei [15–17], performed in the framework of the TANGRA project, in this work we measured the yields and angular distributions of γ -quanta in reactions of the $(n, X\gamma)$ type, where X is n' , $2n$, p , d or α .

2 Experimental setup

The TANGRA setup can be used with different multifunctional γ -detector system configurations. To study different properties of the nuclear reactions occurring upon irradiation with 14.1 MeV neutrons, two detector systems were used: the “Romasha” system with 18 $\text{Bi}_4\text{Ge}_3\text{O}_{12}$ (BGO) detectors and a system with a single ORTEC GMX30-83-PL-S high-purity germanium (HPGe) detector.

The scheme of the TANGRA setup for studying the fast neutron scattering reactions with the HPGe detector is shown in Fig. 1. The HPGe γ -detector was used to obtain high-resolution energy spectra. It has a diameter of 57.5 mm and

a thickness of 66.6 mm. The detector was located at the minimum possible distance from the sample, which excluded direct tagged neutrons from entering the detector. To reduce the background from non-tagged neutrons and to protect the detector from damage by fast neutrons, a lead shielding was used.

The scheme of the TANGRA setup for γ -quanta angular distribution measurements based on BGO detectors is shown in Fig. 2. The “Romasha” system consists of 18 BGO-scintillator γ -detectors placed with 14° step on a circle of radius of 75 cm with the sample in the center. The iron target was placed at a distance of about 75 cm from the floor and about 4 m from the walls. The nearest object containing iron is the neutron generator and the HPGe detector support. It is difficult to separate the background from the generator in the analysis, but it should be practically completely absorbed by the collimator of the HPGe detector. Geometrically, the tagged beams do not hit the detector support.

The portable neutron generator ING-27, produced by VNIIA (Moscow, Russia), is used as a neutron source. It has a built-in 64-channel silicon α -detector, with 8 strips in both horizontal and vertical directions, which forms 64 tagged neutron beams with an energy of 14.1 MeV. The neutrons are produced in the reaction



The reaction (1) is induced by the continuous deuteron beam with kinetic energy from 80 to 100 keV, focused on a tritium-enriched target. The products of this reaction are a 14.1 MeV neutron and a 3.5 MeV α -particle. The α -particles are registered by the 64-pixel α -detector with a pixel dimensions of $6 \times 6 \text{ mm}^2$. The α -detector is located at a distance of 10 cm from the tritium-enriched target. In our experiment only 4 vertical strips were used, the estimated width (FWHM) of a

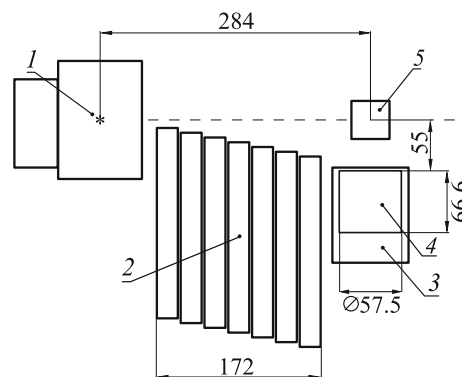


Fig. 1 Scheme of the TANGRA setup with the HPGe detector in the reaction plane: 1 is for the neutron generator ING-27, 2 for the lead shielding, 3 for the case of the HPGe detector, 4 for the HPGe crystal, 5 – sample. Axis of the experimental setup is indicated by horizontal dashed line. Tritium-enriched target is marked as asterisk. All dimensions are given in millimeters

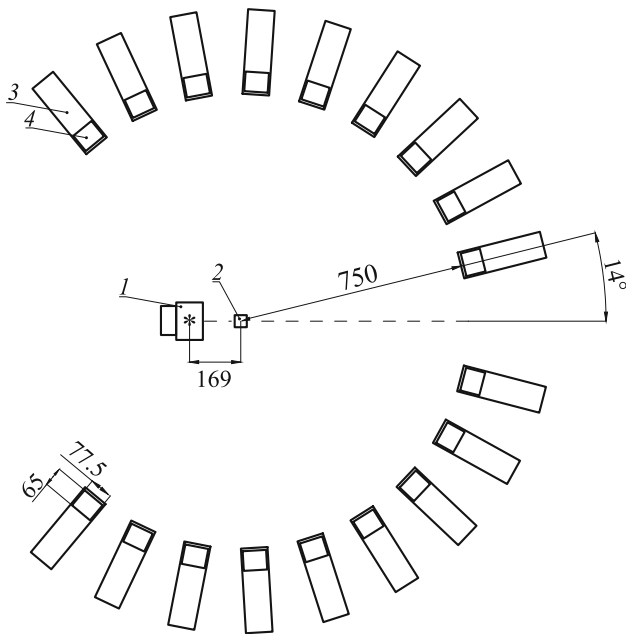


Fig. 2 Scheme of the TANGRA setup with BGO detectors in the reaction plane: 1 is for the portable neutron generator ING-27, 2 for the sample at the center of the “Romasha” γ -ray registration system, 3 for the case of the BGO detector, 4 for the BGO crystal. The symmetry axis of the experimental setup is indicated by horizontal dashed line. The tritium-enriched target is marked by an asterisk. All dimensions are given in millimeters

single neutron beam from single strip at the sample center is 13 mm, the height is 193 mm. The height of the sample (14 cm) was smaller than the height of the tagged neutron beams (19.3 cm). It does not influence our results on the relative yields and angular distributions of the γ -rays, and the absolute cross-sections were not determined.

The TNM is based on registration of the 3.5 MeV α -particle from the reaction (1). The α -particle has practically the opposite direction of flight relative to the direction of the neutron emission. This property allows us to determine the neutron emission direction. The maximal intensity of the total neutron flux in 4π -geometry is $5 \times 10^7 \text{ s}^{-1}$. The α -particles are registered in coincidence with the pulses from the characteristic nuclear γ -radiation, emitted from neutron-induced reactions on the nuclei A in the sample:



So, it is possible to reconstruct the neutron flight direction by estimation of the α -particle emission angle, i.e. to “tag” the neutron. The α - γ coincidence allows one to decrease significantly the number of background events in the γ spectra. Application of the TNM to the data obtained from these two types of the detector systems was quite different.

The background events are separated by using the Time-of-Flight (TOF) method. The TOF is defined as the time difference between the signal from a pixel (or strip) of the

alpha detector and the signal from a γ /neutron detector. The events from neutron-induced reactions on the target form an α - γ coincidence peak in the TOF spectrum, “sitting” on a flat background of random coincidences. In the experiment with HPGe detector because of the small distance and low time resolution this peak contains both γ -rays and secondary neutrons emitted from the target. In the experiment with the “Romasha” BGO detectors the time-of-flight method allows one to separate γ -rays from scattered neutrons (Fig. 3). All signals were recorded by the data acquisition based on 32-channel 100 MHz digitizers [18]. These devices cannot digitize long pulses such as signals from HPGe, so another digitizer CRS-6 was used to collect the data from HPGe detector. The profiles of the tagged neutron beams were measured prior to the experiment, using a position-sensitive silicon charged particle detector for fast neutron detection via the $^{28}\text{Si}(n, \alpha)$ reaction [19]. This information was used for adjusting the neutron generator beams and for the samples’ sizes optimization. The experimental data analysis procedure is discussed in detail in our previous paper [15].

The dimensions of the irradiated sample were chosen from two contradictory requirements: the sample size must allow us to use as many tagged beams as possible, but, on the other hand, the self-absorption of γ -quanta inside the sample must not significantly change the observed γ -quanta angular dis-

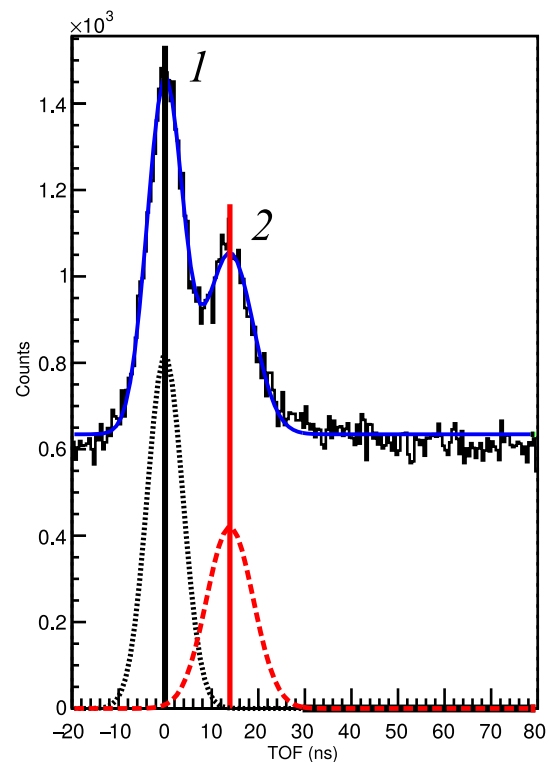


Fig. 3 An example of the TOF spectrum for the BGO detector. Peak 1 corresponds to γ -quanta emitted from the sample, peak 2 to scattered neutrons

tribution. The simplicity of the sample preparation was also an important factor, so we decided to use a box-shaped containers for powders of different chemical compositions. The iron powder chemical purity is about 99%.

We used a Geant4-based Monte-Carlo simulation to estimate the influence of the γ -quanta and neutron absorption inside the sample. The simulation results showed that the optimal sample shape has a square section in the detector plane. The correction coefficients were calculated for each combination of α - γ detectors and applied in the analysis. For all tagged beams used, the distortion of the observed anisotropy of γ -radiation in the case of the selected container size does not exceed 20%. The difference between the angular distributions for different pixels on the same vertical strip was found to be insignificant, so, we decided to use all 8 pixels on the vertical strip, and the height of the sample was set equal to 14 cm. The sample used was a $4 \times 4 \times 14 \text{ cm}^3$ container made of 0.2 mm aluminum foil and filled with pure natural (^{56}Fe -91.75%, ^{54}Fe -5.85%, ^{57}Fe -2.12%) iron powder with a density of 3.53 g/cm^3 . These sample dimensions allowed us to use 4 vertical strips: the two central beams were used for the determination of yields and angular distributions, the other two beams did not cover the sample completely and were used for estimation of the radiation background in the collected γ -spectra. To determine the background component in the γ -spectra resulting from the interaction of neutrons with the sample holder and other structural materials of the setup, a separate measurement was performed with an empty box.

All detectors were calibrated using standard γ -radiation sources. For BGO scintillation detectors the light output and, accordingly, the energy calibration are not very stable and depend on the temperature, load, and other external factors. Considering these features of the BGO detectors, an additional real-time calibration was applied using known background lines recorded during the measurement with the sample.

3 Data analysis

To realize the tagged neutron method, two different approaches were used. In the case of measurements with the BGO detectors, the TOF-based event separation was performed to select events, which are connected with nuclear reactions inside the sample. The time resolution of the BGO γ -detectors lies between 7.5 and 8.6 ns and it is enough to separate the scattered neutrons and γ -quanta.

In Fig. 3 an example of the TOF spectrum is presented. A 2σ time window around the γ -peak was taken to fill the gated γ -spectrum. This approach decreases the number of background events that leads to removing the substrate and background peaks from the final spectrum; the number of the neutron events inside the gamma window depends on

the relative position of the γ -detector and neutron beam and does not exceed 25% for detectors placed close to the direct beam (these data points were rejected) and 12% for used $n - \gamma$ combinations. For each tagged neutrons strip and γ detector combination the contribution of the neutron events was determined from the TOF spectra. The energy spectra of the neutron events were also determined in the neutron time window and subtracted from the energy spectra in the gamma window, after proper normalization. A slightly different method was used to process the data obtained with HPGe detector. In this case it is not possible to separate γ -quanta and neutrons from the sample due to low time resolution of the HPGe detector. Due to the strong dependence of the HPGe detector time resolution on the event energy [20], a special procedure is needed to select a proper time window for each γ -ray energy and then improve background separation and prevent loss of good events.

To obtain events, which are mostly correlated with reactions inside the sample, we approximated the peak centroid in the TOF-energy spectrum (Fig. 4) and selected a window with 3σ width around that peak. We call that time interval the coincidence window. According to our estimation, after the above described procedure the HPGe time resolution in different energy ranges is between 26 ns (in the energy interval 600–900 keV) and 17 ns (in the interval 3600–3900 keV). The energy resolution of the HPGe detector in our experiment was 0.8% for the strongest observed γ -line 846.8 keV and 0.6% for the γ -line 1238.3 keV. The coincidence peak σ at energies of 1000–1300 keV is 9.5 ns, the signal from direct neutrons in the bottom part of the neutron beam hitting the floor should arrive ≈ 60 ns, and from walls about 90 ns later than from the sample. These events are subtracted as anticoincidences. The neutrons scattered at about 90° could hit the HPGe detector and contribute to the background, but their impact could be separated due to the good energy resolution of the HPGe detector. In the case of the measurements with the BGO detector system additional measurement with empty box was made to estimate the γ spectrum generated by

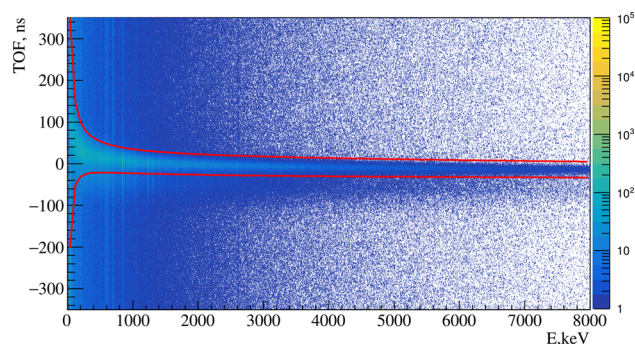


Fig. 4 Full TOF-energy spectrum from measurement with the HPGe detector. The time gate is marked by solid lines

the scattered neutrons in the facility elements and it was taken into account in the data processing procedure. Moreover, in the γ -spectra obtained in experiments with other samples, the peaks of iron are not observed, which indicates that the γ -quanta emitted in reactions on the iron contained in the surrounding materials practically do not affect the obtained coincidence spectra.

After this procedure the number of registered events, which correspond to the γ -ray emission from different discrete states of nuclear reaction products, could be extracted from the γ -spectra. To obtain these values, the full energy absorption peaks were approximated by gaussians with linear background.

We use thick samples in our experiments, which leads to the absorption of the γ -rays and neutrons in the sample and to a non-homogeneous distribution of the γ -ray emission points. In our data processing, corrections for the absorption of neutrons and γ -quanta were not calculated separately. Due to the fact that the tagged neutron beams have a rather complex spatial distribution and the neutrons are absorbed and scattered inside the sample, the subsequent γ -ray emission inside the sample also turns out to be inhomogeneous. Because of this, instead of the absorption coefficients, the ratio

$$\epsilon(E) = \frac{A_{G4}}{N_{G4\gamma}} \quad (3)$$

was introduced for each neutron beam, where N is the calculated in Geant4 number of γ -quanta emitted during neutron–nuclear reactions and A is the calculated number of registered γ -quanta. Thus, $\epsilon(E)$ takes into account both the absorption of neutrons by the sample and the self-absorption of γ -quanta, as well as the efficiency of the γ -detector. The yields of the individual γ -lines were determined from the areas under the corresponding gaussians:

$$Y_{\gamma}(E_i) = \frac{N_{\gamma}(E_i)\epsilon(E_0)}{N_{\gamma 0}(E_0)\epsilon(E_i)} * 100\%. \quad (4)$$

The index $i = 0$ corresponds to the most intense observed γ -transition, to which all other lines are normalized. The values of $\epsilon(E)$ for the two strips used lie between 0.0085 at 100 keV and 0.001 near 4 MeV; for 846.8 keV they are 0.0022 and 0.0030, for 1238.3 keV they become 0.0018 and 0.0023. The difference between calculated and measured efficiency of the γ -detectors does not exceed 20% and a correction factor was added to the $\epsilon(E)$ values.

To measure the γ -ray angular distribution an array of BGO γ -spectrometers was used. Figure 5 shows the comparison between the experimental γ -ray spectra obtained in coincidence with tagged neutrons using the BGO detectors and the HPGe detector.

In the case of measurements with BGO detectors, due to their low energy resolution, the so-called response function

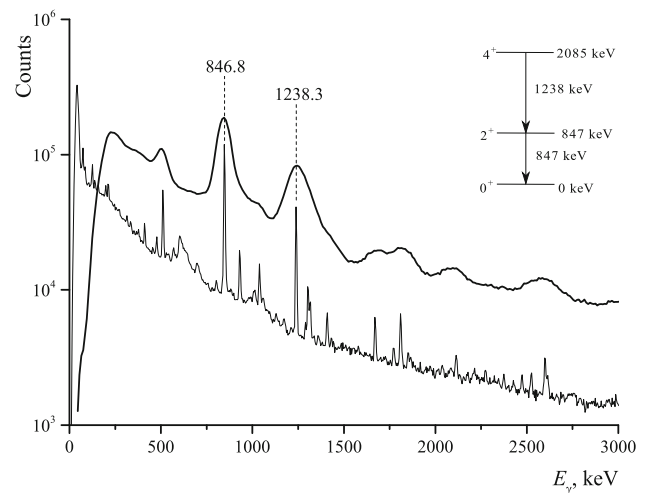


Fig. 5 Gamma-spectra for iron, obtained with “Romasha” BGO and HPGe γ -detector systems

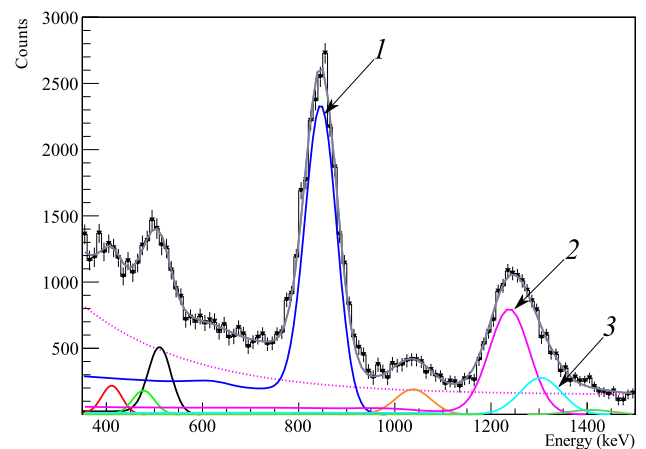


Fig. 6 An example of the BGO spectra analysis. The experimental points are obtained after the random coincidence background subtraction. Solid colored lines represent the response functions of individual γ -transitions. The dashed line corresponds to a smooth additional background substrate. Peak 1 corresponds to the 846.8 keV line, peak 2 to 1238.3 keV, peak 3 is formed by 1289.5, 1303.4 and 1316.4 keV γ -rays

was used, which includes the full energy absorption peak, single- and double-escape peaks, and Compton continuum. The energy spectra for each BGO detector were fitted by the sum of the response functions of all characteristic lines plus additional smooth background substrate. The contribution of background from untagged neutrons was determined from the anticoincidence spectra and subtracted with proper normalization. An example of such a fit is shown in Fig. 6. The details of the response function are discussed in [21].

The parameters of the angular distributions of γ -quanta relative to the direction of the incident neutron beam were determined. Since the energy resolution of BGO detectors does not allow one to separate efficiently the peaks of the

total absorption of the γ quanta of close energies, the angular distributions were determined only for the strongest γ -transitions. The situation shown in Fig. 6 is quite indicative: the peak at an energy of 1238.3 keV is distorted due to overlap with a nearby peak. The sum response function takes into account all peaks, and in the case when they are too close to each other the uncertainties of their areas increases. The minimization procedure performs the function behavior analysis near minimum and determines the errors of the parameters automatically. The relative probabilities of the emission of γ -quanta of a given energy at one angle were determined from the area under the corresponding gaussian. The necessary corrections for the absorption of γ -rays in the sample, as well as the effective solid angles for each detector, were obtained as a result of modeling in Geant4.

The differential cross-section of the γ -ray emission can be represented as

$$\frac{d\sigma_\gamma}{d\Omega} = \frac{\sigma_\gamma}{4\pi} W(\theta), \quad (5)$$

where σ_γ is the γ -ray emission cross-section for a given γ transition; $W(\theta)$ is the angular distribution function.

In our data the procedure measuring the angular distribution $W^{exp}(\theta)$ was obtained by normalization of the measured full energy absorption peak area:

$$W_i^{exp} = \frac{A_i}{\langle A \rangle}, \quad (6)$$

where A_i is the γ -peak area in the detector i and $\langle A \rangle$ is the average full energy absorption peak area. After that the calculated angles with the Geant4 code for each α -strip- γ -detector combination were assigned to W_i^{exp} . To take into account the absorption of γ -quanta inside the sample, the correction coefficients K_i were calculated using Geant4:

$$K_i^{G4} = \frac{A_i^{G4}}{\langle A^{G4} \rangle} \quad (7)$$

where A_i^{G4} is the Geant4-calculated γ -peak area, $\langle A^{G4} \rangle$ is the average peak area. These correction factors were applied to the experimental data using the relation

$$W_i = \frac{W_i^{exp}}{K_i} \quad (8)$$

where K_i is a correction coefficient, which is specific for each α -strip- γ -detector combination. For all used samples, the values of K_i were between 0.7 and 1.3. Figure 7 shows that the correction procedure removes a significant left-right anisotropy caused by different distances from the γ -ray

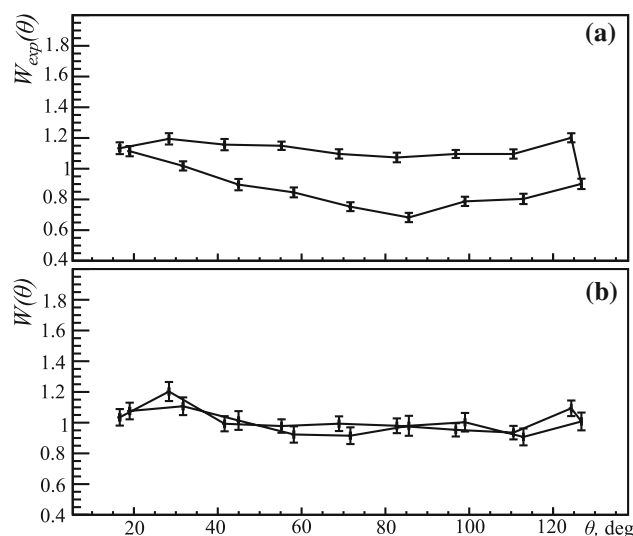


Fig. 7 Data processing example: experimental data $W^{exp}(\theta)$ (set of W_i^{exp}) before correction (a) and corrected angular distribution (set of W_i) (b) for 846.8 keV γ -line

emission volume to the left and right parts of the BGO detector system. The obtained angular distributions of γ -quanta are usually approximated with a series of Legendre polynomials:

$$W(\theta) = A \left(1 + \sum_{k=2,4,\dots}^{2J} a_k P_k(\cos \theta) \right) \quad (9)$$

where A is the normalization coefficient, a_k are expansion coefficients, J is the γ -transition multipolarity.

4 TALYS 1.9 calculations for ^{56}Fe

The main advantage of TALYS software is its versatility: it includes modern descriptions of main reaction mechanisms (direct, compound, multi-step, and fission) and covers a wide range of energies (up to 200 MeV) and target nuclei [23]. This software can be used for the verification of ranges where the theoretical approaches are valid. On the other hand, in its development, TALYS also turns into a tool for generating nuclear data in areas where these data are difficult to obtain experimentally. These applications require the default parameter sets to be in regular checking and “fine-tuning” modes.

The TALYS software has become an important component in the study of neutron-induced reactions in a wide range of energies. Several years ago the program code TALYS 1.6 was successfully used to describe the experimental results on inelastic neutron scattering by iron isotopes [6, 8, 10]. In our model calculations, we use a more recent version of the TALYS 1.9 code [24].

For optical model and for coupled-channel calculations TALYS software includes ECIS-06 [25] as a subroutine. The optical model calculation, based on the global Koning–Delaroche parametrization, is adjusted to the neutron total cross-section data for ^{56}Fe and neutron differential scattering data in the energy range from 4 to 26 MeV [26]. In Table 1 the values of optical potential parameters for several incident energies E_n are shown. To illustrate the parameters' energy dependence, we provide parameter sets for three energies E_n : a low energy of 2.0 MeV, relevant for TANGRA experiment energy of 14.1 MeV and the highest one used in the calculations, 20.0 MeV. In vibrational model and rotational model calculations, the imaginary surface parameter W_D was reduced by 15% compared to the values indicated in the Table 1, the other parameters had the same values. The notation agrees with Ref. [26].

We compared the obtained experimental cross-section data from other papers with nuclear reaction code TALYS calculations to check its applicability to γ -ray emission cross-section evaluation and test its sensitivity to the model parameters' variation.

By default, in TALYS 1.9 the calculation is conducted in the distorted-wave Born approximation (DWBA), therefore the ^{56}Fe nucleus is considered to be near-spherical. At the same time noticeable deformation is indicated in TALYS 1.9 by the default parameters. For the first excited state of ^{56}Fe , $\beta_2 = 0.239$. Coulomb-excitation studies lead to almost the same $\beta_2 = 0.2393 \pm 0.0049$ for ^{56}Fe isotope [27]. This is a relatively large value, and thus the direct collective reactions are significant. For higher excitation levels β_2 did not exceed the value of 0.065. In this work the same TALYS 1.9 default values of β_2 for the excited states were accepted in all calculations, parameters β_λ with $\lambda > 2$ were considered zero valued because β_2 plays a leading role.

Compared with DWBA a more adequate description of the experimental results on inelastic neutron scattering by the ^{56}Fe isotope at E_n from 1.5 to 26 MeV was obtained using coupled-channel (CC) calculations [10,28]. Better agreement of the results of the coupled-channel calculations with the experimental 2_1^+ excitation cross-section at 6.96 and 7.96 MeV projectile kinetic energy was obtained in [10] with $\beta_2 = 0.24$.

In this work, besides the default, TALYS 1.9 calculations using the CC method with rotational and vibrational

models were conducted. In the rotational model the lowest $0^+, 2^+, 4^+$ excited states in ^{56}Fe were coupled in rotational band. In the vibrational model the lowest $0^+, 2^+$ levels were coupled, and the 2^+ level was considered a one-quadrupole phonon excitation.

TALYS 1.9 can be used to calculate cross-sections of processes taking place in a nuclear reaction. Using calculated cross-sections it is possible to deduce other reaction characteristics. In this work we calculated the individual γ -line yields $Y(E_i)$:

$$Y(E_i) = \frac{\sigma_k(E_i)}{\sigma_p^{max}} \cdot \frac{\nu_k}{\nu_p} \tag{10}$$

where $\sigma_k(E_i)$ is the cross-section of the γ -transition, resulting from the reaction on the isotope k , σ_p^{max} is the cross-section of the most intense γ -transition, resulting from the reaction on the isotope p , ν_k , and ν_p are the abundances of the isotopes k and p , respectively. In the case of an iron sample, the normalization was made to the cross-section for the transition $E_\gamma = 846.8$ keV ($2_1^+ \rightarrow 0_{gs}^+$) for the isotope ^{56}Fe . Before performing a yield calculation it is necessary to ensure that TALYS 1.9 is able to describe γ -transition cross-sections in good agreement with the experimental data. Especially it concerns the cross-section value of the most intense γ -transition because it participates in every yield by definition (10).

In order to check the quality of the reproduction of γ -quanta transition cross-sections on iron isotopes by the TALYS 1.9 software, we calculated the cross-sections for the range of E_n from 0.1 MeV to 20 MeV with a step of 0.1 MeV. In Fig. 8, the cross-sections of emitting the γ -quanta with $E_\gamma = 846.8, 1238.3$ keV as a function of E_n are showed. Note that TALYS was not intended for describing the resonance region; that is why TALYS does not reproduce the fine structure of γ -emission in the low energy region. It is seen that TALYS 1.9 produces the results close to experiment for a wide range of incident neutron energies E_n . Near the energy of our interest, $E_n = 14.1$ MeV, the experimental partial cross-section of γ -quanta with energy $E_\gamma = 846.8, 1238.3$ keV are close to TALYS 1.9 results. The model calculations for $E_n = 14.1$ MeV almost lie within the error bars of the cross-sections. At the same time, the calculated cross-sections for the first $2_1^+ \rightarrow 0_{gs}^+$ transition are systematically lower than the evaluated cross-sections.

Table 1 Default spherical optical model potential parameters used in the TALYS 1.9 calculations for neutron energies $E_n = 2, 14.1, 20$ MeV. Depths V_i, W_i of potential components are given in MeV, diffuseness parameters a_i and radii parameters r_i are given in fm

E_n MeV	V_V	r_V	a_V	W_V	W_D	r_D	a_D	V_{SO}	r_{SO}	a_{SO}	W_{SO}
2.0	52.33	1.186	0.663	0.26	6.29	1.282	0.532	5.83	1.00	0.580	-0.02
14.1	47.91	1.186	0.663	1.03	7.67	1.282	0.532	5.55	1.00	0.580	-0.07
20.0	45.86	1.186	0.663	1.55	7.23	1.282	0.532	5.42	1.00	0.580	-0.10

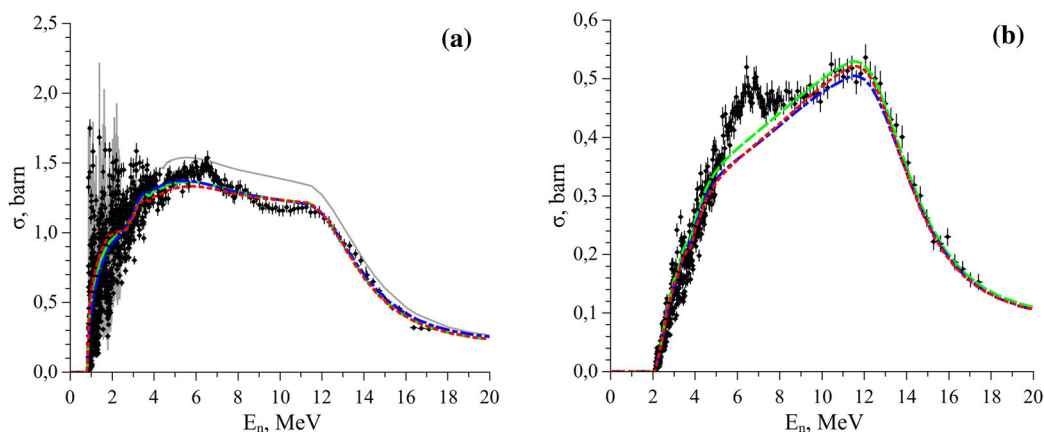


Fig. 8 γ -emission cross-sections for the 846.8 keV γ -ray ($2_1^+ \rightarrow 0_{gs}^+$) (a) and for the 1238.3 keV γ -ray ($4_1^+ \rightarrow 2_1^+$) (b). Shown are a comparison between experimental data from [6] (points), evaluated data

from ENDF.B-VIII.0 database [22] (grey solid line), calculations using TALYS 1.9 with DWBA (red dotted line), vibrational approximation (blue dashed-dotted line), and rotational approximation (green dashed line)

This difference reaches a maximum bigger than 0.2 mb near $E_n = 5$ MeV and grows close to 0.1 mb around $E_n = 14.1$ MeV.

It is difficult to conclude which applied model describes the experimental data better. All three curves of TALYS calculation results are mostly overlapping in Fig. 8, integral cross-sections received in vibrational, rotational, and DWBA methods do not show significant difference. The question of the most appropriate model for the ^{56}Fe nucleus was discussed in the previous work [28]. Furthermore, in calculations of the γ -line yields $Y(E_i)$ the DWBA integral cross-sections were used.

The model calculations for the energy dependencies of the partial cross-sections for formation of γ -quanta, in general, are in good agreement with the experimental data. Calculated integral cross-sections seem to be appropriate to use in Eq. (10).

5 Results

We used a HPGe γ -spectrometer to obtain a high-resolution γ -spectrum. 19 γ -transitions from $^{56}\text{Fe}(n, X)$ reactions were observed with a sufficient number of events to identify γ -transition and extract the yield with a good accuracy. They are marked in the spectrum in Fig. 9. The main properties of these transitions are listed in Table 2. The table also shows the yields obtained in our experiment in comparison with the results from the calculation using the TALYS code and experimental data from other work [11, 33]. Due to statistical limitations we present the measured data for which the γ -production cross-section ≥ 10 mb.

As the natural iron sample contains the isotope ^{57}Fe , the total production cross-section for the 846.8 keV γ -ray on ^{nat}Fe includes, above $E_n = 8.64$ MeV, a component from the $^{57}\text{Fe}(n, 2n)^{56}\text{Fe}$ reaction. The detailed analysis of this contribution was made in [6, 7]. The abundance of ^{57}Fe is 2.12(3)% [1], so the impact of the $^{57}\text{Fe}(n, 2n)^{56}\text{Fe}$ reaction should be small (according to the TALYS calculation it is about 3%). Despite the small value of the contribution, at an incident neutron energy in the region of 14 MeV, its presence creates certain difficulties in determining the cross-section of the most intense γ -line with $E_\gamma = 846.86$ keV. The calculated cross-sections of this γ -transition in comparison with the experimental data are shown in Table 3. There is a difference between the calculated absolute cross-sections and those from the compilation [11], but the calculated value lies between experimentally determined values used for data estimation. A general analysis of the uncertainties for the major reaction channels for ^{56}Fe in the fast neutron range is given in Ref. [37].

A comparison of the measured and estimated from [11] γ -ray yields shows that the discrepancy between them does not exceed 16% for γ -transitions with intensity $> 9\%$ and 30% for transitions with yield $> 5\%$. The experimental and estimated data comparison with TALYS shows agreement better than 30% with our yields and better than 35% with the compilation [11] for the γ -transition with intensity $> 5\%$. It is important to notice that the largest discrepancies between TALYS and the experimental data are for $^{56}\text{Fe}(n, 2n)^{55}\text{Fe}$ and $^{54}\text{Fe}(n, n')^{54}\text{Fe}$ reactions, so the default parameters of the optical potential in TALYS for ^{55}Fe and ^{54}Fe should be adjusted.

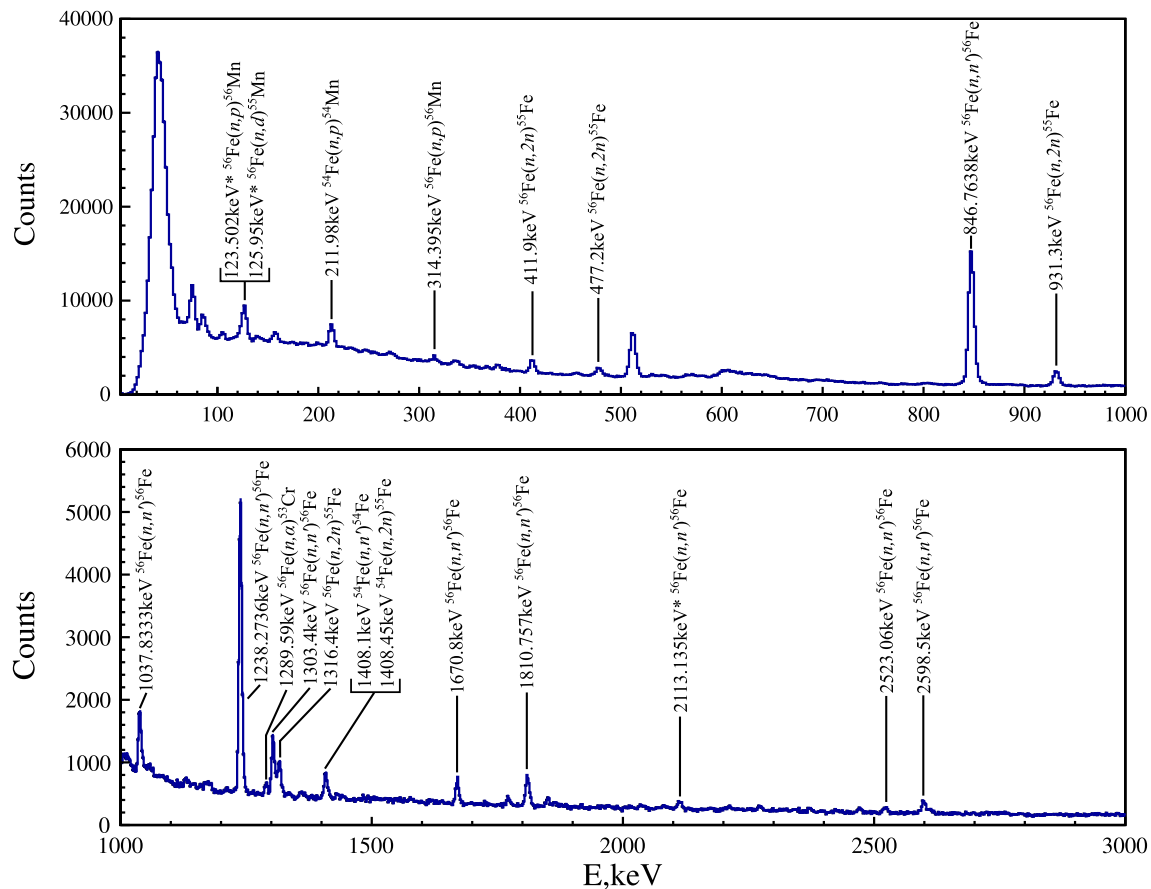


Fig. 9 Gamma-spectrum for Fe (HPGe). Energies of the most intense γ -transitions E_γ (in keV) from reactions $^{56}\text{Fe}(n, n')$, $(n, 2n')$, (n, p) , (n, d) , (n, α) are signed. Energies matching observables' peaks are taken from NDS [29–32]

The γ -quanta angular distributions for Fe have been measured using the “Romasha” γ -spectrometer system. In Fig. 5 the γ -spectrum obtained by the BGO γ -detectors is shown. We present the γ -quanta angular distributions for the two most intense γ -transitions: 847 keV and 1238 keV, which correspond to excitations of the 847 keV(2^+) and 2085 keV(4^+) levels. The measured γ -quanta angular distributions and their approximations are shown in the Fig. 10 in comparison with the other experimental results [34–36]. The corresponding coefficients of the Legendre polynomial approximation are given in Table 4. The discrepancy between the data from different experiments is not large for the 847 keV γ -line in the 45° – 150° angular range, at low angles the points are overlapping within the margins of errors except the data from [34]. The data points for 1238 keV γ -rays from our experiment and [34–36] are close to each other, except for two data points from [34] at small angles. Such systematical deviation of 15° and 30° data may be a consequence of the peculiarities of the data processing procedure in [34]. In Refs. [35,36] the errors of the data fit are not presented, so we have made our approximation for them.

The comparison of the angular distribution coefficients shows a significant discrepancy in the coefficient a_2 for 847 keV transition. Our results are close to [34], our coefficient a_2 is smaller than the one in [34,35]. Our approximation shows that the coefficient a_4 is insignificant for this transition.

For the 1238 keV γ -transition the situation is quite similar. Our value a_2 is smaller than the one in [34,35], the coefficient a_4 is insignificant for this transition according to the data from [35,36] and important according to our data.

The obtained values correspond to the main trends of the energy dependences of the angular distribution coefficients obtained evaluating the cross-sections and angular distributions of γ -quanta in neutron scattering reactions on iron for E_n from 0.5 to 19 MeV [38]: for the 846.8 keV γ -transition the a_2 -value is clearly positive and a_4 is mainly negative. Above 2 MeV the angular distribution flattens out and the a_4 value is close to zero. In [38] it was noted that for the γ -line $E_\gamma = 1238.3$ keV the coefficient a_4 is small, therefore $a_4 = 0$ was assumed in the analysis. The recent results of the n ELBE experiment [9] in the range of initial neu-

Table 2 Parameters of the γ -transitions observed in this work. The asterisk “*” marks γ -lines that cannot be separated. Energies of γ -quanta E_γ and the level parameters J_i^P , J_f^P were taken from NDS, Adopted levels [29–32]. For the energies measured in this work statistical uncertainties only are presented. For each γ -line spin–parity J^P

and energy E for the initial (i) and the final (f) levels are given. The measured yields of γ -transitions Y_γ are compared with TALYS 1.9 calculation results and the experimental data from [33] and the compilation [11]

E_γ , keV this work	NDS	Reaction	Initial state $J_i^P(E_i, \text{keV})$	Final state $J_f^P(E_f, \text{keV})$	Y_γ , % this work	TALYS	[11]	[33]
123.5(4)*	123.5	$^{56}\text{Fe}(n, p)^{56}\text{Mn}$	5^+ (335.5)	4^+ (212.0)	6(1)	5.8		
126.0(4)*	126.0	$^{56}\text{Fe}(n, d)^{55}\text{Mn}$	$\frac{7}{2}^-$ (125.9)	$\frac{5}{2}^-$ (0)				
211.9(2)	212.0	$^{54}\text{Fe}(n, p)^{54}\text{Mn}$	5^+ (368.2)	4^+ (156.3)	5.9(8)	4.81		
	212.0	$^{56}\text{Fe}(n, p)^{56}\text{Mn}$	4^+ (212.2)	0^+ (0)				
335.7(5)	335.5	$^{56}\text{Fe}(n, p)^{56}\text{Mn}$	3^+ (341.0)	2^+ (26.6)	2.2(8)	1.04		
411.2(2)	411.9	$^{56}\text{Fe}(n, 2n)^{55}\text{Fe}$	$\frac{1}{2}^-$ (411.4)	$\frac{3}{2}^-$ (0)	5.3(7)	7.05	6.8(8)	
477.4(5)	477.2	$^{56}\text{Fe}(n, 2n)^{55}\text{Fe}$	$\frac{7}{2}^-$ (1408.5)	$\frac{5}{2}^-$ (931.3)	4.6(7)	3.97	6.4(9)	
846.86(2)	846.8	$^{56}\text{Fe}(n, n')^{56}\text{Fe}$	2^+ (846.8)	0^+ (0)	100.0(6)	100	100	100
		$^{57}\text{Fe}(n, 2n)^{56}\text{Fe}$						
931.4(1)	931.3	$^{56}\text{Fe}(n, 2n)^{55}\text{Fe}$	$\frac{5}{2}^-$ (931.3)	$\frac{3}{2}^-$ (0)	12.0(8)	19.43	10.7(9)	15(5)
1038.1(2)	1037.8	$^{56}\text{Fe}(n, n')^{56}\text{Fe}$	4^+ (3123.0)	4^+ (2085.1)	8.2(8)	6.48	6.0(5)	10(2)
1238.53(4)*	1238.3	$^{56}\text{Fe}(n, n')^{56}\text{Fe}$	4^+ (2085.1)	2^+ (846.8)	43.8(1.1)	49.90	36(2)	46(5)
		$^{57}\text{Fe}(n, 2n)^{56}\text{Fe}$						
1289.7(5)	1289.6	$^{56}\text{Fe}(n, \alpha)^{53}\text{Cr}$	$\frac{7}{2}^-$ (1289.5)	$\frac{3}{2}^-$ (0)	1.7(5)	1.68		
1304.0(1)*	1303.4	$^{56}\text{Fe}(n, n')^{56}\text{Fe}$	6^+ (3388.6)	4^+ (2085.1)	9.2(6)	9.89	9.3(6)	10.1(1.5)
		$^{57}\text{Fe}(n, 2n)^{56}\text{Fe}$						
1316.0(2)	1316.4	$^{56}\text{Fe}(n, 2n)^{55}\text{Fe}$	$\frac{7}{2}^-$ (1316.5)	$\frac{3}{2}^-$ (0)	5.6(5)	8.65	6.8(8)	7.4(1.2)
1408.3(3)*	1408.1	$^{54}\text{Fe}(n, n')^{54}\text{Fe}$	2^+ (1408.2)	0^+ (0)	4.0(6)	6.50	3.0(6)	5.7(1.2)
	1408.5	$^{56}\text{Fe}(n, 2n)^{55}\text{Fe}$	$\frac{7}{2}^-$ (1408.5)	$\frac{3}{2}^-$ (0)				
1670.6(2)	1670.8	$^{56}\text{Fe}(n, n')^{56}\text{Fe}$	6^+ (3755.6)	4^+ (2085.1)	4.5(5)	5.1	6.9(7)	6.3(1.2)
1810.7(2)	1810.8	$^{56}\text{Fe}(n, n')^{56}\text{Fe}$	2^+ (2657.6)	2^+ (846.8)	6.7(5)	3.27	4.8(6)	7.7(1.2)
		$^{57}\text{Fe}(n, 2n)^{56}\text{Fe}$						
2114.2(6)	2113.1	$^{56}\text{Fe}(n, n')^{56}\text{Fe}$	2^+ (2960.0)	2^+ (846.8)	2.5(7)	1.8	1.9(6)	4.5(1.2)
2524.2(8)	2523.1	$^{56}\text{Fe}(n, n')^{56}\text{Fe}$	2^+ (3370.0)	2^+ (846.8)	2.5(7)	1.37	2.7(6)	
2600.3(5)	2598.5	$^{56}\text{Fe}(n, n')^{56}\text{Fe}$	3^+ (3445.3)	2^+ (846.8)	3.4(5)	2.07	4.5(6)	

tron energies between 0.1 and 7 MeV confirm the main conclusions; however, the obtained experimental information for five different γ -lines indicates the necessity of taking angular distribution effects of higher orders into account. In [9] for the 1238.3 keV γ -ray angular distribution positive a_2 and negative a_4 are observed over the entire energy range.

6 Summary

Using TANGRA facility and the tagged neutron method, we determined the γ -radiation parameters from the inelastic interaction of 14.1 MeV neutrons on natural iron. The data obtained are generally consistent with the known literature data, but some significant differences are observed for

Table 3 The cross-sections of the 846.86 keV γ -line emission (mb) from the calculations with TALYS software and from the compilation of experimental data [11,33]

Reaction	TALYS	[11]	[33]
$\text{natFe}(n, n' + 2n)$	621.92	785(48)	663(70)
$^{56}\text{Fe}(n, n')^{56}\text{Fe}$	656.94	621(29)	
$^{57}\text{Fe}(n, 2n')^{57}\text{Fe}$	904.58	–	

some lines. For the most intense lines, the angular anisotropy parameters of the emission of γ -quanta relative to the direction of the neutron beam are determined. The comparison of the measured yields with the calculated one shows a large discrepancy for the $(n, 2n)$ reactions, so this information could be used to improve the model description of the neutron-

Fig. 10 The angular distributions of the γ -quanta from 14.1 MeV neutron inelastic scattering on ^{56}Fe versus scattering angle θ in c.m. system: $E_\gamma = 847$ keV (a), $E_\gamma = 1238$ keV (b). Experimental data: solid circles are for this work, triangles are for [34], squares are for [35], empty circles for [36]. The line is a Legendre polynomial fit of the data, measured in this work

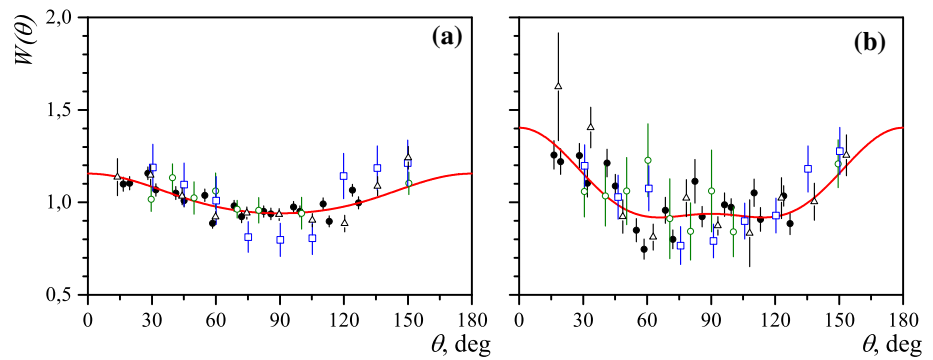


Table 4 Legendre polynomial approximation coefficients for the γ -quanta angular distributions obtained in this work in comparison with previous measurements

E_γ keV	a_2	a_4	Reference
846.8	0.13(2)	0.02(2)	This work
	0.21(5)	0.07(3)	[34]
	0.36	-0.38	[35]
	0.09	-0.1	[36]
1238.3	0.24(4)	0.16(6)	This work
	0.32(8)	0.16(8)	[34]
	0.37	-0.23	[35]
	0.14	-0.1	[36]

induced reactions. The difference in the angular anisotropy coefficients obtained in different experiments probably is connected with issues of the neutron background estimation at low angles, so measurement with high-resolution detectors is required to solve this problem.

Funding This work was partially supported by JINR AYSS grant 20-402-07. This work was partially supported by JINR AYSS grant 20-402-03.

Data Availability Statement This manuscript has no associated data or the data will not be deposited. [Authors' comment: The datasets generated during and/or analysed during the current study are available from the corresponding author on reasonable request.]

References

- J. Meija et al., Pure Appl. Chem. **88**, 293 (2016)
- NEA Nuclear Data High Priority Request List, <https://www.oecd-nea.org/dbdata/hprl/>
- The CIELP Project, <https://www-nds.iaea.org/CIELO/>
- D.E. Lea, Proc. R. Soc. Lond. A **150**, 637 (1935)
- C.M. Castaneda et al., Nucl. Instrum. Methods B **260**, 508 (2007)
- A. Negret et al., Phys. Rev. C **90**, 034602 (2014)

- A. Negret et al., Phys. Rev. C **96**, 024620 (2017)
- R. Beyer et al., Nucl. Phys. A **927**, 41 (2014)
- R. Beyer et al., Eur. Phys. J. A **54**, 58 (2018)
- A.P.D. Ramirez et al., Phys. Rev. C **95**, 064605 (2017)
- S. Simakov et al., *INDC(CPP)-0413* (IAEA Nuclear Data Section, Vienna, 1998)
- V. Valković, *14 MeV Neutrons. Physics and Applications*, 1st ed. (Taylor & Francis Group, Boca Raton, 2016)
- V.M. Bystritsky et al., Phys. Part. Nucl. Lett. **12**, 325 (2015)
- I.N. Ruskov et al., Phys. Proc. **64**, 163 (2015)
- D.N. Grozdanov et al., Phys. Atom. Nucl. **5**, 588 (2018)
- N.A. Fedorov, D.N. Grozdanov, V.M. Bystritsky et al., Eur. Phys. J. Web of Conf. **177**, 02002 (2018)
- N.A. Fedorov et al., Phys. Atom. Nucl. **82**, 343 (2019)
- AFI electronics, <http://afi.jinr.ru>
- N. Zamyatin et al., Nucl. Instrum. Methods A **898**, 46 (2018)
- F.C.L. Crespi, V. Vandone, S. Brambill et al., Nucl. Instr. and Meth. A **620**, 299 (2010)
- D.N. Grozdanov et al., Indian J. Pure Appl. Phys. **58**, 427 (2020)
- D.A. Brown et al., Nucl. Data Sheets **148**, 1 (2018)
- A.J. Koning et al., Nucl. Data Sheets **155**, 1 (2019)
- A.J. Koning et al., *Proceedings of the International Conference on Nuclear Data for Science and Technology, April 22–27, 2007, Nice, France*, editors O. Bersillon, F. Gunsing, E. Bauge, R. Jacqmin, and S. Leray, EDP Sciences, p. 211–214 (2008)
- J. Raynal, CEA Saclay report CEA-N-2772, Notes on ECIS94 (1994)
- A.J. Koning et al., Nucl. Phys. A **713**, 231 (2003)
- S. Raman, C.W. Nestor, P. Tikkanen, At. Data Nucl. Data Tables **78**, 1 (2001)
- A.B. Smith, Nucl. Phys. A **605**, 269 (1996)
- H. Junde, H. Su, Y. Dong, Nucl. Data Sheets **112**, 1513 (2011)
- H. Junde, Nucl. Data Sheets **110**, 2689 (2009)
- H. Junde, H. Su, Y. Dong, Nucl. Data Sheets **109**, 787 (2008)
- H. Junde, H. Su, Nucl. Data Sheets **107**, 1393 (2006)
- R.O. Nelson et al., Los Alamos Scientific Lab. Reports, No.02-7167 (LA-UR-02-7167), USA (2002)
- A.P. Dyagterev, Yu.E. Kozyr, G.A. Prokopec, *Proceedings of the 4th All-Union Conference on Neutron Physics, Kiev, 1977*, edited by L.N. Usachev, Vol. 2 (Atominform, Moscow, 1977)
- U. Abbondanno et al., J. Nucl. Energy **27**, 227 (1973)
- J. Lachkar et al., Nucl. Sci. Eng. **55**, 168 (1974)
- M. Herman et al., Nucl. Data Sheets **148**, 214 (2018)
- M.V. Savin et al., J. Nucl. Sci. Tech. Suppl. **1**, 748 (2000)